Inorg. Chem. **2002**, *41*, 3269–3279

Cooperative Ligation, Back-Bonding, and Possible Pyridine–Pyridine Interactions in Tetrapyridine–Vanadium(II): A Visible and X-ray Spectroscopic Study

Patrick Frank,[†,‡] Phalguni Ghosh,[†,§,||] Keith O. Hodgson,*[,†,‡] and Henry Taube*[,‡]

Department of Chemistry, Stanford University, Stanford, California 94305, Stanford Synchrotron Radiation Laboratory, SLAC, Stanford University, Stanford, California 94309, and Parker Hughes Cancer Center, St. Paul, Minnesota 55113

Received November 30, 2001

The binding of pyridine by V(II) in aqueous solution shows evidence for the late onset of cooperativity. The K_1 governing formation of $[V(py)]^{2+}$ ($\lambda_{max} = 404$ nm, $\epsilon_{max} = 1.43 \pm 0.3$ M^{-1} cm^{-1}) was determined spectrophotometrically to be 11.0 ± 0.3 M^{-1}, while K_1 for isonicotinamide was found to be 5.0 ± 0.1 M^{-1}. These values are in the low range for 3d M^{2+} ions and indicate that V(II)·py back-bonding is not significant in the formation of the 1:1 complex. Titration of 10.5 mM V(II) with pyridine in aqueous solution showed an absorption plateau at about 1 M added pyridine, indicating a reaction terminus. Vanadium K-edge EXAFS analysis of 63 mM V(II) in 2 M pyridine solution revealed six first-shell N/O ligands at 2.14 Å and 4 ± 1 pyridine ligands per V(II). UV/vis absorption spectroscopy indicated that the same terminal V(II) species was present in both experiments. Model calculations showed that in the absence of back-bonding only 2.0 ± 0.2 and 2.4 ± 0.2 pyridine ligands would be present, respectively. Cooperativity in multistage binding of pyridine by $[V(aq)]^{2+}$ is thus indicated. XAS K-edge spectroscopy of crystalline $[V(O_3SCF_3)_2(py)_4]$ and of V(II) in 2 M pyridine solution each exhibited the analogous $1s \rightarrow {}^5E_g$ and $1s \rightarrow {}^5T_{2g}$ transitions, at 5465.5 and 5467.5 eV, and 5465.2 and 5467.4 eV, respectively, consistent with the EXAFS analysis. In contrast, $[V(py)_6](PF_6)_2$ and $[V(H_2O)_6]SO_4$ show four $1s \rightarrow 3d$ XAS transitions suggestive of a Jahn–Teller distorted excited state. Comparison of the M(II)–N_{py} bond lengths in V(II) and Fe(II) tetrapyridines shows that the V(II)–N_{py} distances are about 0.06 Å shorter than predicted from ionic radii. For $[VX_2(R\text{-}py)_4]$ ($X = Cl^-$, $CF_3SO_3^-$; R = 4-Et, H, 3-EtOOC), the $E_{1/2}$ values of the V(II)/V(III) couples correlate linearly with the Hammett σ values of the R group. These findings indicate that π back-bonding is important in $[V(py)_4]^{2+}$ even though absent in $[V(py)]^{2+}$. The paramagnetism of $[V(O_3SCF_3)_2(py)_4]$ in $CHCl_3$, 3.8 ± 0.2 μ_B, revealed that the onset of back-bonding is not accompanied by a spin change. Analysis of the geometries of V(II) and Fe(II) tetrapyridines indicates that the ubiquitous propeller motif accompanying tetrapyridine ligation may be due to eight dipole interactions arising from the juxtaposed C–H edges and π clouds of adjoining ligands, worth about –6 kJ each. However, this is not the source of the cooperativity in the binding of multiple pyridines by V(II) because the same interactions are present in the Fe(II)–tetrapyridines, which do not show cooperative ligand binding. Cooperativity in the binding of pyridine by V(II) is then assigned by default to V(II)–pyridine back-bonding, which emerges only after the first pyridine is bound.

In an earlier publication, the spectrophotometric properties of species of the formula $[VX_2(py)_4]$ where "py" is pyridine and X is a mononegative ion or of species $[V(py)_4L_2]X'_2$ where L is a neutral molecule and X′ is a weakly nucleophilic anion (PF_6^- or BPh_4^-) in pyridine as a solvent were reported.[1] The intense absorptions observed in the visible electronic spectra are ascribable to $\pi d \rightarrow \pi^*$ (ligand) charge transfer

* Authors to whom correspondence should be addressed. H.T.: fax, 650-725-0259; tel, 650-725-9344; e-mail, cdpiercy@stanford.edu. K.O.H.: fax, 650-926-4100; tel, 650-723-1328 (Stanford University), 650-926-3153 (Stanford Synchrotron Radiation Laboratory); e-mail, Hodgson@ssre.slac.stanford.edu.

† Department of Chemistry, Stanford University.

‡ Stanford Synchrotron Radiation Laboratory, SLAC, Stanford University.

§ Parker Hughes Cancer Center.

|| Present address: Department of Medicinal Chemistry, University of Minnesota, Minneapolis, MN 55455.

(1) Ghosh, P.; Taube, H.; Hasegawa, T.; Kuroda, R. *Inorg. Chem.* **1995**, *34*, 5761−5775.

10.1021/ic011221o CCC: $22.00
Published on Web 05/23/2002

transitions, and to d−d transitions of enhanced intensity due to the influence of the four π-acceptor ligands. The intensity of the metal-to-pyridine transitions might suggest that M·L back-bonding plays a role in $[V(py)_4]^{2+}$, which is not unexpected when taking into account the electronic structure of the ion (πd^3) and the fact that $[V(aq)]^{2+}$ is a strong reducing agent. This proposal is strongly reinforced by the respective V(III)/V(II) reduction potentials for $[V(O_3SCF_3)_2(py')_4]$ in pyridine solution, which are -0.17 ± 0.01 V, 0.0 ± 0.01 V, and 0.27 ± 0.01 V vs NHE for py′ = 4-ethylpyridine, pyridine, or ethylnicotinate.[1] The trend reflects a decreasing stabilization of the 3+ oxidation state relative to the 2+ as the electron-withdrawing power of the pyridines increases. If only σ-inductive effects were operative, the same general trend would be expected because the higher vanadium oxidation state will be stabilized most by the strongest nucleophile, namely, 4-ethylpyridine. However, the calculated difference of 10^8 in the relative binding constants is much too great to be accounted for on this basis. Therefore, stabilization of the lower oxidation state relative to the higher by an additional factor is indicated. We take this factor to be back-bonding because the effects will be greatest for ethylnicotinate, as observed.

However, the affinity of the pyridines for V(II) in the first stage of association showed no evidence for back-bonding.[1] Late appearance of back-bonding suggests cooperativity in the formation of the multicomplexed V(II)−pyridine species. In prominent examples of such cooperativity, most frequently illustrated by the reaction of $[Fe(aq)]^{2+}$ with a strong π-electron acceptor, there is a change from high spin to low spin in the course of the stepwise displacement of H_2O by the ligand. For example, the K_1, K_2, and K_3 values governing the formation of tris-complexation of $[Fe(aq)]^{2+}$ are 7.3×10^5, 1.78×10^5, and 1.1×10^{10} for 1,10-phenanthroline, and 1.6×10^4, 5×10^3, and 3.6×10^{10} for 2,2′-bipyridyl.[2] In the case of bipyridyl, the conclusion for cooperativity was confirmed by Davies and Dunning.[3] The causal connection between the change in spin state and cooperativity in binding is also made in at least two deservedly influential textbooks.[4,5]

In this paper we report the results of the spectrophotometric measurements, referred to in the earlier paper,[1] of the affinity of pyridine for $[V(aq)]^{2+}$ in the first stage of association. The nature of the fully complexed V(II) species in 2 M aqueous pyridine was determined by EXAFS analysis. The source of cooperativity in pyridine binding by V(II) is assessed in terms of the structure and electronic state, including spin magnetism, of the tetrapyridine complex. Comparisons are made with the isostructural $[Fe(py)_4]^{2+}$ complex, which does not form cooperatively. In the course of this analysis, we propose a new rationale for the ubiquitous propeller motif in metal tetrapyridines. The spin change associated with the cooperative binding of *o*-phenanthroline or 2,2′-bipyridyl by $[Fe(aq)]^{2+}$ is suggested to be a consequence of the emergence of back-bonding, the actual source of cooperativity in reaction of the aqua ions of 3d transition metals with π-acceptor ligands. On this account, the observations we have made have at least didactic significance.

Materials and Methods

The compounds $[V(O_3SCF_3)_2(py)_4]$, $[V(O_3SCF_3)_2(THF)_4]$, and $[V(py)_6](PF_6)_2$ were prepared as described.[1] $[V(H_2O)_6]SO_4$ was prepared using the procedure of Cotton et al.[6] Pyridine and 1,5-pentanediol were reagent quality. UV/vis spectra were recorded in a quartz cell or cuvette on either a Hewlett-Packard model 8452A diode array spectrophotometer or a Beckman model 5270 spectrophotometer.

All spectrophotometric samples were prepared in an argon-filled glovebox (<1 ppm of O_2). For the titration of V(II) with pyridine, the appropriate amount of solid $[V(O_3SCF_3)_2(THF)_4]$ (light blue crystals) was dissolved in 5.00 ± 0.05 mL of deionized water and aliquots of pyridine were sequentially added using a Hamilton gastight syringe. The initial concentration of the hexaaqua species was checked using the extinction coefficients of the two well-resolved low-energy d−d transitions detected at 843 nm ($\epsilon = 4.5$ M^{-1} cm^{-1}) and 556 nm ($\epsilon = 4.3$ M^{-1} cm^{-1}), respectively.[7] UV/vis spectra of the V(II)/pyridine solutions were collected after 15 min of stirring. In a typical Hildebrand titration experiment 15.1 ± 0.1 mg of crystalline $[V(O_3SCF_3)_2(THF)_4]$ was dissolved in 5.00 ± 0.05 mL of deionized water to generate 4.74 mmol/L of pink-violet $[V(H_2O)_6]^{2+}$ solution. To this solution was added 1.00 μL of pyridine using a Hamilton gastight 5 μL syringe to obtain 2.47 mmol/L concentration in the bulk. The mixture was stirred well for 15 min at 24.6 °C before the charge transfer band was monitored at 404 nm. After each measurement, the mole ratio of vanadium to pyridine was increased by the addition of more solid $[V(O_3SCF_3)_2(THF)_4]$ and the reaction mixture was stirred as before. A constant ionic strength of the medium was maintained with a 0.3 M solution of $NaCF_3SO_3$ salt.

The magnetic moment of $[V(CF_3SO_3)_2(py)_4]$ was determined by the Evans method.[8] In a typical experiment 0.010 g $[V(O_3SCF_3)_2(py)_4]$ was dissolved in 1.5 g of $CHCl_3$ and transferred to an NMR tube that contained an inner concentric tube containing only the solvent. The data were treated by use of the equation $\chi = 3\Delta/4\pi\nu c + \chi_g$. Here, Δ is the separation of the two solvent signals, ν the frequency of the NMR spectrophotometer (300.1008 MHz), c the concentration in g/mL, and χ_g the gram susceptibility of $CHCl_3$, which is -0.497×10^{-6} cgs/g. Diamagnetic corrections for the solute were made by recourse to Pascal constants.

All XAS sample preparations were carried out in a dinitrogen-filled glovebox (Vacuum Atmospheres, Hawthorne, CA) operating at 1 ppm dioxygen or better. Vanadium(II) as a 63 mM solution in 2.0 M aqueous pyridine with 40% 1,5-pentanediol was prepared directly by dissolution of an appropriate weight of $[V(O_3SCF_3)_2(THF)_4]$ in the named solvent. Absorption spectra and the first derivatives of these spectra showed that the V(II) species in pyridine/40% aqueous 1,5-pentanediol was the same as that in aqueous pyridine alone. All sample solutions were dispensed and handled using Hamilton gastight microliter syringes. Vanadium K-edge XAS spectra were obtained at the Stanford Synchrotron Radiation Laboratory (SSRL) on wiggler beamline 7-3 under

(2) Irving, H.; Mellor, D. H. *J. Chem. Soc.* **1962**, 5222−5237.
(3) Davies, R. L.; Dunning, K. W. *J. Chem. Soc.* **1965**, 4168−4185.
(4) Basolo, F.; Pearson, R. G. *Mechanisms of Inorganic Reactions in Solution*; John Wiley & Sons: New York, 1967; p 23.
(5) Cotton, F. A.; Wilkinson, G. *Advanced Inorganic Chemistry*, 5th ed.; Wiley-Interscience: New York, 1988; pp 44, 45.
(6) Cotton, F. A.; Falvello, L. R.; Llusar, R.; Libby, E.; Murillo, C. A.; Schwotzer, W. *Inorg. Chem.* **1986**, *25*, 3423−3428.
(7) Jørgensen, C. K. Spectroscopy of Transition-Group Complexes. In *Advances in Chemical Physics*; Prigogine, I., Ed.; Interscience: New York, 1963; Vol. v, pp 33−146.
(8) Evans, D. F. *J. Chem. Soc.* **1959**, 2003−2005.

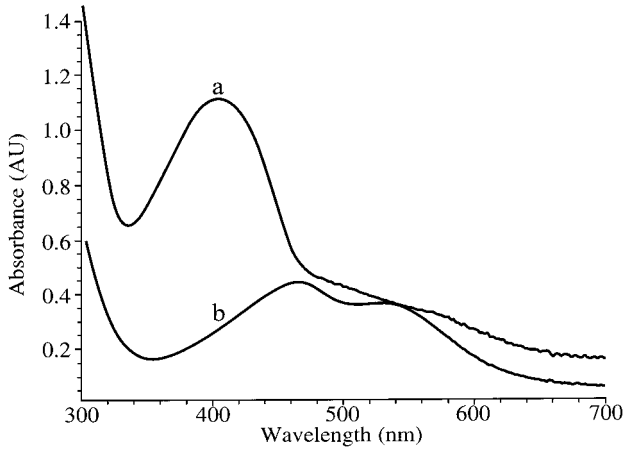

Figure 1. The limiting UV/visible absorption spectrum of (a) the titration of 2.48 mM pyridine with V(II); [V(II)] is 66.7 mM; (b) the titration of 1.64 mM isonicotinamide with V(II); [V(II)] is 30.0 mM.

dedicated operating conditions of 60−90 mA at 3 GeV, and with a wiggler field of 18 kG. The X-ray beam was energy resolved using a Si[220] double crystal monochromator and was detuned 50% at 6337 eV to minimize harmonic contamination. Solid samples were finely dispersed in boron nitride prior to data collection, and X-ray spectra were measured by transmission using an in-line nitrogen-filled detector. Solution samples were contained in 2 mm path length Lexan sample cells, and X-ray spectra were obtained using an argon-filled Stern−Heald−Lytle fluorescence detector set at 90° from the incident beam. All X-ray spectra were measured at 10 K using an Oxford Instruments CF1208 continuous flow liquid helium cryostat. Data were calibrated relative to a vanadium foil standard. For transmission samples, vanadium foil reference spectra were collected concomitantly. For solution samples, vanadium foil reference spectra were separately collected from time to time during data acquisition. Vanadium K-edge XAS spectra were calibrated relative to the first rising inflection of the K-edge XAS spectrum of vanadium foil, set to 5464.0 eV. EXAFS data were fit using FEFF7 within the program XFPAKG, written by Dr. Graham George of SSRL. The data were fit only over the range 3−11 in *k*-space, due to the presence of ice-crystal diffraction spikes in the data at higher *k*.

Results

In order to assess the appearance of late-stage cooperativity in the binding of pyridine by V(II), it was necessary to determine the association constant for the formation of $[V(py)]^{2+}$. To obtain K_1 the absorption in the visible range of the spectrum is followed as a function of the increasing concentration of V(II), while the total concentration of pyridine remains low and constant. At greater concentrations of V(II), the contribution to the absorption by complexes of higher order is reduced, and in the limit of very high V(II) concentration, only the 1:1 complex is observed. The UV/vis spectrum of the 1:1 complex, shown in Figure 1, has an absorption maximum at 404 nm and a shoulder at longer wavelengths and, in general, resembles the spectra observed for tetrapyridine species as determined in pyridine as a solvent.[1]

To estimate the value of K_1 and ϵ_1, the extinction coefficient for the 1:1 complex, the titration data were treated by the method of Hildebrand,[9] as in eq 1,

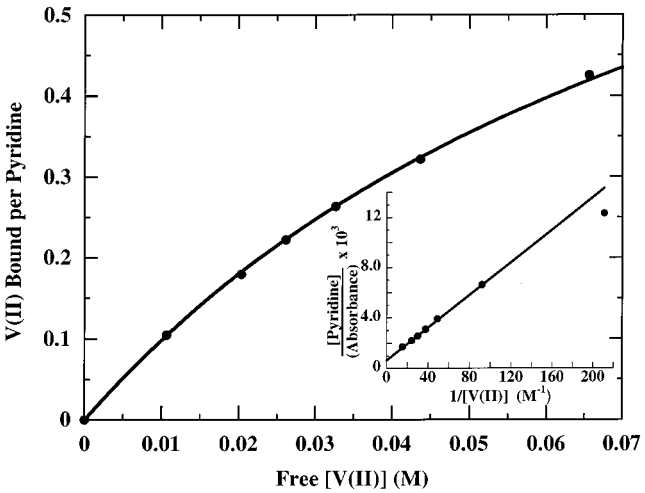

Figure 2. Data points showing the titration of 2.48 mM pyridine with V(II) in water solution. (—) The fit to the data using the equation $K_1[V(II)]_{free}/(1 + K_1[V(II)]_{free})$ describing a simple equilibrium. Inset: A Hildebrand plot of the data. The line is the linear least-squares fit ($y = 6.83 \times 10^{-4} + 6.48 \times 10^{-5}x$; $r = 0.9997$) to the first six points. See text for details.

$$[Py]_0/A = 1/\epsilon_1 K_1[V(II)] + 1/\epsilon_1 \quad (1)$$

where $[Py]_0$ is the fixed total concentration of pyridine, A is the absorbance corresponding to a particular value of the variable $[V(II)]^{-1}$, and the other variables are defined as above. In a plot of $[Py]_0/A$ vs $1/[V(II)]$, the slope of the line is given by $1/\epsilon_1 K_1$, and the intercept by $1/\epsilon_1$. The data at low values of ($[V(II)]^{-1}$) are favored because an increase in the concentration of V(II) reduces the contribution of complexes of higher order to the total absorbance. These, if present, result in a negative deviation from the linear progression of the values of $[Py]_0/A$. If cooperative binding is a factor at the concentration of pyridine chosen, the effect of the deviation due to higher-order complexes is exaggerated. Valid Hildebrand data thus produce a linear plot, and this is shown in Figure 2, inset. Here, the point for the lowest concentration of $[V(aq)]^{2+}$ used, $1/[V^{2+}] = 210\ M^{-1}$, showed a negative deviation and so was omitted from the linear fit. (Figure 1, Supporting Information, shows the successive UV/vis traces with a constant total concentration of pyridine as the concentration of V(II) increases.)

Least squares treatment of these data ($r = 0.9997$) led to a value of $10.7 \pm 0.2\ M^{-1}$ for K_1 and $1.43 \pm 0.03 \times 10^3\ M^{-1}\ cm^{-1}$ for the extinction coefficient of the 1:1 complex, the latter to be compared to $2.6 \times 10^3\ M^{-1}\ cm^{-1}$ for $[V(py)_4]^{2+}$ in 2.0 M aqueous pyridine. Using the value of the extinction coefficient derived from the Hildebrand treatment of the data, a titration plot was constructed and was then fit using the equation $y =$ number of V(II) ions bound per mole of pyridine $= K_1 \times [V(II)]_{free}/(1 + K_1[V(II)]_{free})$.[10,11] This fit ($r = 0.9998$) is shown in Figure 2 and yielded $K_1 = 11 \pm 0.3\ M^{-1}$ for the first V(II)−pyridine binding constant. In an attempt at replication, K_1 was

(9) Benesi, H. A.; Hildebrand, J. H. *J. Am. Chem. Soc.* **1949**, *71*, 2703−2707.
(10) Klotz, I. M. *Acc. Chem. Res.* **1974**, *7*, 162−168.
(11) Klotz, I. M.; Hunston, D. L. *J. Biol. Chem.* **1984**, *259*, 10060−10062.

measured as 10 ± 1 M^{-1}, the corresponding value of ϵ_1 being $1.3 \pm 0.1 \times 10^3$ M^{-1} cm^{-1}. These data were clearly inferior, showing much more point scatter, and we settle on 11.0 M^{-1} and 1430 M^{-1} cm^{-1} as the values of K_1 and ϵ_1.

Isonicotinamide is a stronger π acceptor than pyridine, and the preference for this ligand is enhanced when the metal ion can act as a πd electron donor. Following the analogous Hildebrand experiment a similar treatment of the data ($r = 0.998$) yielded $K_1 = 5.0 \pm 0.1$ M^{-1} and $\epsilon_1 = 1.74 \pm 0.4 \times 10^3$ M^{-1} cm^{-1} at $\lambda_{max} = 465$ nm. What was a low-intensity shoulder at longer wavelength for pyridine now appears as a well-defined maximum at 538 nm, and so the absorption spectrum for the 1:1 V(II)−isonicotinamide complex, Figure 1, trace b, differs significantly from that observed for pyridine. (Supporting Information Figure 2 shows the successive absorption spectra resulting from the Hildebrand titration of isonicotinamide with increasing [V(II)].)

Ethylisonicotinate is also a stronger electron acceptor than pyridine, and with it as ligand again two well-defined peaks are observed, that appearing at 535 nm being almost as intense as the higher energy band at 475 nm. Because of the limited solubility of the ester in water, accurate values of K_1 were not obtained, but it is certain that the value is lower than that obtained for pyridine.

The trend in K_1 values suggests that back-donation does not play a significant role in the first stage of association in the binding of pyridine ligands to $[V(aq)]^{2+}$. This conclusion is strongly reinforced by comparison with the corresponding 1:1 association constants of other 3d M^{2+} ions for pyridine in aqueous solution (in units of M^{-1}): Fe^{2+}, 4 ± 0.9; Co^{2+}, 14 ± 0.3; Ni^{2+}, 60 ± 1; Cu^{2+}, 260 ± 6; and Zn^{2+} 7.6 ± 0.2, respectively.[12,13] Despite the fact that $[V(aq)]^{2+}$ is a much stronger reducing agent than any of these dipositive ions, the value of K_1 for pyridine ligation is in the lower range of those listed. However, there is evidence for cooperativity during multiple ligations of $[V(aq)]^{2+}$ by pyridine.

Thus, treatment of V(II) with increasing concentrations of pyridine, monitored by absorption spectroscopy, produced a titration curve that reached a plateau just above 1.00 M total pyridine, as shown in Figure 3. As will be described below, application of XAS spectroscopy showed that the plateau values correspond to about four pyridines per V(II) arranged to yield a tetragonal complex. The values of the equilibrium constants for three or four successive stages of association of $[Co(aq)]^{2+}$, $[Ni(aq)]^{2+}$, $[Cu(aq)]^{2+}$, and $[Zn(aq)]^{2+}$ with pyridine have been determined, and they all decrease monotonically, indicating the absence of cooperativity.[13] In order to estimate the number of pyridines that would be bound per V(II) in the absence of cooperativity under the experimental conditions, we approximated the equilibrium constants K_{2-4} for $[V(aq)]^{2+}$ by scaling K_1 for $[V(aq)]^{2+}$, namely, 11 M^{-1}, by the known equilibrium constants K_1-K_4 governing the Ni^{2+}−pyridine system.[13] Comparison of $[V(aq)]^{2+}$ with $[Ni(aq)]^{2+}$ is particularly appropriate because the electronic structure of Ni(II) similarly

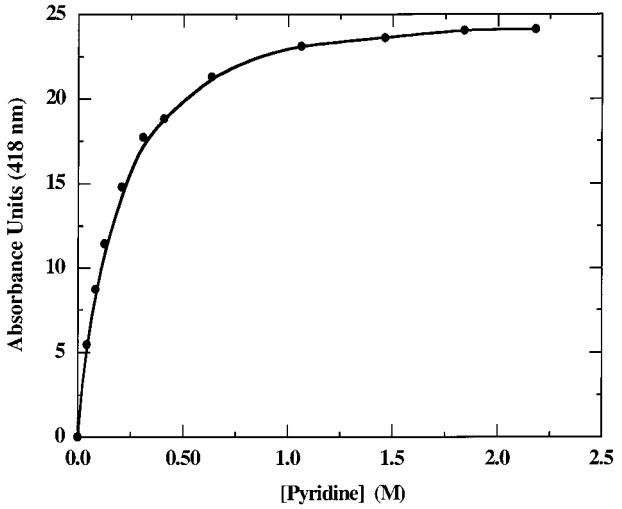

Figure 3. Titration plot of 10.5 mM V(II) in aqueous solution with increasing concentrations of pyridine. The limiting absorbance is reached just above 1.00 M total pyridine. The line is an arbitrary curve drawn through the data points.

consists of three d electrons of the same spin but now embedded in a spherically symmetrical distribution of five d electrons of opposite spin. Beyond K_4, the values of K_5 and K_6 for V^{2+} were estimated by applying the statistical factors to the calculated value of K_4 for V^{2+}, which overestimate the affinities.[14] This approach is reasonable because of the electronic analogy between V^{2+} and Ni^{2+} noted above, and provides a generous upper limit for the noncooperative binding of pyridine to V^{2+} because Ni^{2+} has a relatively higher charge density.[15] In addition, in the absence of confounding effects, the successive values of the equilibrium constants typically decline more rapidly than if dictated by the statistical factors alone. For example, the decline in K_4 compared to K_1 resulting from the statistical factor alone is 8.0, while the experimental factor deriving from ligation by ammonia of $[Co(aq)]^{2+}$ is 22, and of $[Ni(aq)]^{2+}$ is 41.[13] The upper-limit average number of pyridines associated with the V^{2+} in the absence of cooperativity under the conditions of the Figure 3 experiment was thus calculated to be 2.0 ± 0.2 by the method outlined above. The uncertainty in the calculated result is the standard deviation obtained by propagating the errors in the known Ni(II) binding constants, as percents. While the plateau value is not quite reached at 1 M pyridine, the average value observed using EXAFS is not much less than 4, as shown below. UV/vis spectroscopy verified that the same V(II)−pyridine complex was present in each experiment.

Measurement of the paramagnetism of $[V(O_3SCF_3)_2(py)_4]$ in chloroform solution yielded a value of 3.8 ± 0.2 μ_B (see Materials and Methods section). The observed magnetism is consistent with a quartet ground state, indicating that tetrapyridine ligation is not accompanied by spin pairing. Therefore, any cooperative effect in binding of pyridine by V(II) cannot be ascribed to this cause.[4,5]

(12) Bjerrum, J. *Acta Chem. Scand.* **1973**, *27*, 970−976.
(13) Sundberg, R. J.; Martin, R. B. *Chem. Rev.* **1974**, *74*, 471−517.
(14) Kim, S.-H.; Martin, R. B. *Inorg. Chim. Acta* **1984**, *91*, 19−24.
(15) Shannon, R. D.; Prewitt, C. T. *Acta Crystallogr. B* **1969**, *25*, 925−945.

It should be noted that, in a tetragonal $[V(py)_4]^{2+}$ complex, the maximum benefit from back-bonding is achieved if the four pyridines lie in a plane perpendicular to the *z*-axis. In this configuration a VN_4 molecular orbital can be constructed with only a single node lying in the plane perpendicular to the molecular axis. If the pyridine planes were parallel to the molecular *z*-axis, all the π^* orbitals would remain localized, losing some of the benefit of cooperativity gained by constructing molecular orbitals from independent orbitals. Comparison of the absorption spectrum of $[V(py)]^{2+}$ with that of $[V(O_3SCF_3)_2(py)_4]$ dissolved in pure pyridine is particularly relevant here. Neat pyridine does not significantly displace the anion from the metal, and so in both cases the effects of axially located oxygen donors are being compared. The absorption maximum observed at 404 nm for the 1:1 complex is shifted to longer wavelengths for the tetrapyridine ditriflate, occurring at 424 nm, $\epsilon = 4600\ M^{-1}\ cm^{-1}$. While each pyridine added to the metal increases the work needed to remove an electron, this effect is apparently more than compensated for by the stabilization arising from constructing the lowest lying π^* molecular orbital from those of the four interacting nitrogen centers. The tilt in the planes of the four pyridine rings from the coplanar arrangement represents in part a compromise between the steric repulsion that is maximum in a coplanar arrangement, and loss in the electronic stabilization of back-bonding as the tilt from coplanarity increases. We will return to this point in the Discussion section after description of the XAS results below.

The Fit to the EXAFS Spectrum

EXAFS analysis of 63 mM V(II) in 2 M pyridine solution was carried out to determine the average number of pyridine ligands carried by the metal center under these conditions. Because of ice diffraction features in the EXAFS of the frozen solution spectra collected at 10 K, the data were analyzed only over the range 3−11 in *k*-space. It was anticipated that the ligation sphere of V(II) would consist of a mixture of oxygen and nitrogen atoms under the conditions of 2 M aqueous pyridine solution. Because the photoelectron scattering parameters of bound nitrogen and oxygen atoms are highly similar, it is not possible to distinguish between the contributions each makes to the V(II) K-edge EXAFS spectrum at the resolution of the current experiment. In addition, the expected metrical precision of the EXAFS fit over 3−11 in *k*-space is only about 0.19 Å. For this reason, separate shells of ligands similar in Z and differing in absorber−scatterer distance by as much as 0.2 Å cannot be distinguished, and so the first ligation sphere about V(II) was treated as a single shell of scatterers of one atom type (nitrogen). Therefore, determining the number of pyridine ligands devolved upon determining the number of carbon atoms in any second-shell scattering features.

The Fourier transform EXAFS spectrum of 63 mM V(II) in 2 M pyridine solution is shown in Figure 4. The prominent feature at about $R = 1.85$ Å represents the first ligation sphere of nitrogen/oxygen scatterers. This value is uncorrected for phase shift. At higher values of *R*, features evident at about 2.6 and 3.8 Å clearly indicate the presence of more distant scatterers. These can only arise from the presence of pyridine ligands.

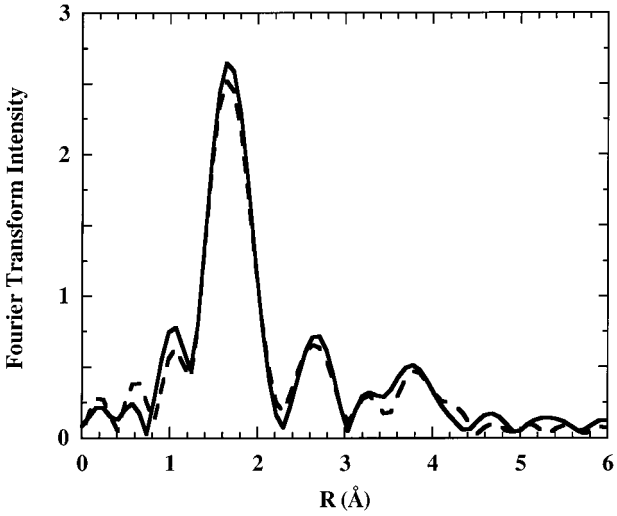

Figure 4. Fourier transform XAS spectrum of (−) 63 mM V(II) with 2 M pyridine in 40% aqueous 1,5-pentanediol; (− − −) the fit to the XAS data.

Fits to the data were carried out using FEFF7, which includes provision for fitting multiple-scattering features. The scattering parameters required by FEFF were obtained using the known crystal structure[1] of $[V(O_3SCF_3)_2(py)_4]$ as the initial model. When pyridine ligands were included in fits, the coordination numbers of second-shell atoms and of multiple-scattering interactions were linked to the number of pyridine ligands. Thus, in a fit with one pyridine ligand, for example, the single-scattering second-shell $V-C_\alpha$ interactions were fixed at 2, as were the $V-C_\beta$ interactions. In no test fits was it found necessary to include a single-scattering interaction between the vanadium absorber and the C_γ of the pyridine ligand. Likewise, for evaluation of multiple-scattering contributions to the EXAFS, for each pyridine ligand the number of, e.g., $V-N-C_\alpha$ interactions was kept fixed at 4.

When the Debye−Waller (DW) values were allowed to float freely during a fit, the FEFF algorithm always found a nominally best fit in which the DW values were negative. Because this result is physically meaningless, in all fits except the final fit, all of the Debye−Waller values were linked and required to reflect the same relative proportion as those calculated by FEFF for the crystalline $[V(O_3SCF_3)_2(py)_4]$ model. In the final fit, the Debye−Waller value of the six V−N/O first-shell interactions was allowed to float freely. The original proportionate linkage among the Debye−Waller parameters of the more distant single- and multiple-scattering shells was retained.

In order to determine the ligation around V(II), the coordination number (CN) of pyridine ligands was stepped between values of 1 and 6. For fits with pyridine CN <6, the remaining first-shell ligands were modeled as isolated O/N scatterers representing water molecules. Nearly equivalently good fits were obtained for every ligand set tested between a low of 1 pyridine ligand with 5 water molecule ligands and a high of 6 pyridine ligands, as judged by the

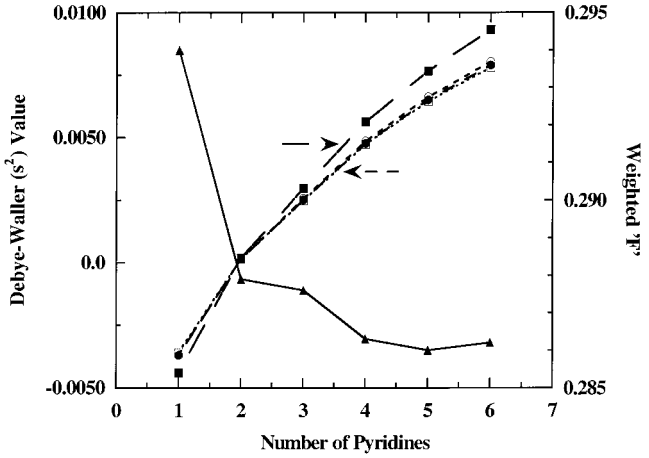

Figure 5. Trends in Debye−Waller (dashed lines, left ordinate) and goodness-of-fit "*F*" (full line, right ordinate) values. The symbols for the Debye−Waller interaction are (●) V−C_α single scattering; (○) V−N−C_α multiple scattering; (■) V−L−L multiple scattering; (□) V−C_α−C_β multiple scattering. Arrows mark the DW values of the $[V(O_3SCF_3)_2(py)_4]$ model as calculated by FEFF7. The calculated DW values for all the V−C interactions in the model were within the range 0.00372 ± 0.00005.

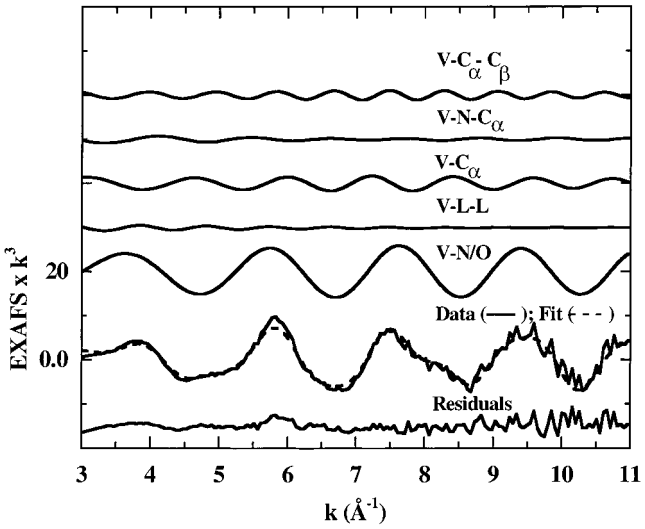

Figure 6. EXAFS data (—) for 63 mM V(II) with 2 M pyridine in 40% aqueous 1,5-pentanediol solvent and (− − −) the fit to EXAFS. The unfit residuals and the components to the fit are labeled on the face of the figure.

intensity of the residuals. However, when the number of pyridine ligands was fewer than 3, the DW values assumed unrealistically low or negative values. Further, the goodness-of-fit parameter "*F*" decreased as the number of pyridines increased through 5 pyridine ligands. The distant-shell DW values also systematically increased with the number of pyridines. Figure 5 shows these trends. The DW values calculated by FEFF for the $[V(O_3SCF_3)_2(py)_4]$ model are also indicated in Figure 5 (arrows). The most reasonable fit was chosen by reference to both "*F*" and the DW values. By the "*F*" criterion, the best fit is about 5 pyridines per V(II).

In further consideration, however, because the DW values for the first shell remained small (0.00230 ± 0.00006) over the entire CN series, disorder in the first-shell distances can be discounted. Consequently, disorder in any carbon second-shell scatterers and multiple-scattering pathways should also be small, because even in solution phase the motions of all the atoms in the pyridine molecule remain correlated. In this case, the DW values associated with longer scattering pathways will also be relatively small and close in value to those for the crystalline model. The only exception to this would be if the pyridine ligands were ruffled about the V(II) center, producing a spread in the respective V−C distances. However, a ligand ruffle is not evident in the crystal structure of $[V(O_3SCF_3)_2(py)_4]$ or any of the $[Fe(py)_4]^{2+}$ complexes discussed here, and so this possibility is unlikely. Thus, the most reasonable fits are those for 3 or 4 pyridine ligands (Figure 5). The DW values for the more distant shells in the CN 4 and 5 fits are comparable to the related pyridine carbons in the well-ordered mixed-metal complex $[Cr_2CoO(CH_3CO_2)_6(py)_3]$,[16] and to those in the rigid tris-catecholate chelate complex $K[Cr(DTBC)_3]$.[17] At 6 pyridine ligands the DW values become unacceptably large relative to the consistently low DW values for the first-shell fit, and are significantly larger than those of the mentioned related complexes. Combining these considerations, the ligation of 63 mM V(II) in 2 M pyridine solution can be assigned to 4 ± 1 pyridines, with the remaining 2 ± 1 ligation sites occupied by water molecules. Under these solution conditions, and in the absence of cooperativity, the upper limit estimate for the average number of pyridines per V^{2+} was calculated to be 2.4 ± 0.2 using the Ni(II)-based method described above. This value is well outside the uncertainty of the EXAFS experiment, reinforcing the conclusion that V(II) binds multiple pyridines cooperatively.

Table 1. Four-Pyridine Fit to the EXAFS of V(II) in 2 M Pyridine Solution

scatterer	CN	distance (Å)	σ^2	ΔE_0	weighted "*F*"
V−N/O ss[a]	6	2.14	0.00226	−6.1434	0.2863
V−L−L[b] ms	12	4.42	0.00563		
V−C_α ss	8	3.10	0.00476		
V−N−C_α ms	16	3.17	0.00485		
V−C_α−C_β ms	16	4.52	0.00473		

[a] "ss" denotes a single-scattering interaction; "ms" denotes multiple scattering. [b] Transverse multiple scattering interaction between ligating first-shell atoms 180° apart.

Figure 6 shows the EXAFS data for 63 mM V(II) in 2 M pyridine solution, the CN = 4 final fit to the data, the components of the fit, and the (data minus fit) residuals. The results of the fit are given in Table 1. The data are well-fit, and the residuals indicate that no periodic contribution to the data remains unfit. After the six first-shell N/O interactions, the largest contribution to the EXAFS was found to be the single-scattering interaction with the eight second-shell pyridine C_α carbons. Nearly as intense is a multiple-scattering interaction between the V(II) absorber and the C_α−C_β carbons on pyridine. Smaller contributions were found for the V−N−C_α multiple-scattering pathway, and the multiple-scattering pathway involving the 12 180° pairwise transverse interactions among the six first-shell atoms, represented by "V−L−L" in Table 1. The latter pathway is nearly in-phase with the V−C_α−C_β multiple-scattering

(16) Edwards, A. B.; Charnock, J. M.; Garner, C. D.; Blake, A. B. *J. Chem. Soc., Dalton Trans.* **1995**, 2515−2519.
(17) Pattison, D. L.; Levina, A.; Davies, M. J.; Lay, P. A. *Inorg. Chem.* **2001**, *40*, 214−217.

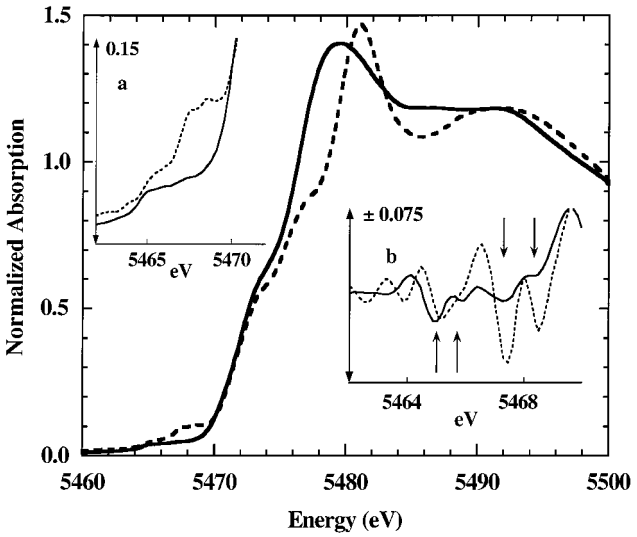

Figure 7. XAS K-edge spectra of (−) crystalline $[V(py)_6](PF_6)_2$ and (− − −), crystalline $[V(H_2O)_6]SO_4$ each finely dispersed in BN. Inset a: Expansion of the preedge energy region of the XAS spectra. Inset b: Second derivative of the data in inset a. In inset b, arrows mark the features corresponding to the 1s → 3d transitions.

pathway, and excluding it made a noticeable deficiency in the fit to the Fourier feature around 3.6 Å in uncorrected "*R*". In Figure 4, comparison of the Fourier transform of the final fit with that of the EXAFS data indicates that all the important features of the data are represented in the fit.

K-Edge Spectra

In Figure 7 are compared the K-edge XAS spectra of crystalline samples of $[V(H_2O)_6]SO_4$ and $[V(py)_6](PF_6)_2$. The symmetry of the hexaaqua complex is virtually pure octahedral, with six V−O distances of 2.130 ± 0.007 Å.[6] In the energy region just below the rising K-edge in XAS spectra of octahedral complexes, the very weak absorption features represent dipole-forbidden, quadrupole-allowed transitions from the 1s level to 3d valence holes.[18] Small departures from pure octahedral symmetry can confer additional intensity on these transitions, however, through d−p mixing.[19] The 1s → 3d transitions therefore carry information about the ligation symmetry of the absorber. K-edge bound-state XAS transitions involving transition metal 1s electrons produce a core-hole and an extra electron in the valence orbitals. Therefore the XAS excited valence-level states of a Z^{n+} ion will resemble the ground and excited optical valence states of a $(Z + 1)^{n+}$ ion. For d^3 V(II), the excited states following promotion of the 1s electron into the 3d manifold will be the d^4 quintet 1s → $^5E_{2g}$ and 1s → $^5T_{2g}$ states similar to those associated with the ground and excited valence states of the homologous $3d^4$ transition metal, Cr(II).

The excited state energy diagram for V(II) following an X-ray 1s → 3d transition is given in Figure 8, in analogy with that of the valence electronic states of d^4 Cr(II).[20] The

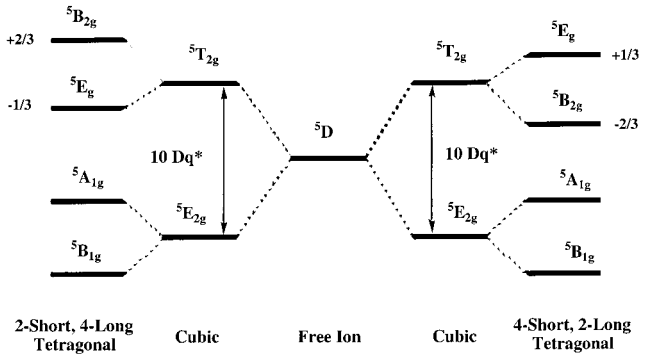

Figure 8. Energy diagram for excited state V(II) following a 1s → 3d X-ray preedge transition indicating the available d^4 quintet states for the Jahn−Teller distorted tetragonal symmetry. The XAS excited state of initially d^3 V(II) is analogous to the $(Z + 1)d^4$ ion Cr(II) (see text). The diagram was adapted from the work of Fackler and Holah.[20]

high-spin d^4 XAS excited state of V(II) will be Jahn−Teller distorted, leading to further splitting of the $^5E_{2g}$ and $^5T_{2g}$ states. Thus, even V(II) complexes that have perfectly octahedral ground states will have K-edge XAS 1s → 3d excited states of tetragonal symmetry, and may display up to four XAS preedge transitions. In Figure 7 inset a, the preedge energy region (5463−5469 eV) of the XAS spectrum of the hexapyridine complex clearly shows at least three transitions, constituting evidence for an excited state of reduced symmetry. The transition features within the XAS preedge spectral energy region of the hexaaqua complex are too weak and too poorly resolved to make this assessment. However, in the second derivatives of the XAS spectra of these complexes (Figure 7, inset b), clear evidence is seen for the four transitions of a Jahn−Teller distorted excited state (arrows).

Inspection of the energy diagram of Figure 8 indicates that the two possible Jahn−Teller ligand arrangements may be distinguished by the relative intensities of the higher energy set of transitions. That is, if the transitions to the ^5E_g and $^5B_{2g}$ states are resolved, the 2-fold degeneracy of the former should produce a more intense transition. For the pyridine complex, the feature at 5467.4 eV in the second derivative of the XAS spectrum is more intense than that at 5468.5 eV, and is associated with a relatively steep rise in absorption intensity (Figure 7, inset a). From Figure 8, this result indicates the likelihood that the excited state Jahn−Teller geometry of $[V(py)_6]^{2+}$ includes two ligands at shorter distance and four at a longer distance. For the hexaaqua complex this also appears to be true, although the poorer resolution due to the low intensities of the features does not permit a confident decision. Howver, the following assignments can be tentatively made, {$[V(H_2O)_6]^{2+}$; $[V(py)_6]^{2+}$}: 1s → $^5B_{1g}$ {5464.9, 5465.1 eV}; 1s → $^5A_{1g}$ {∼5465.8, 5465.9 eV}; 1s → ^5E_g {5467.3, 5467.4 eV}; 1s → $^5B_{2g}$ {5468.4, 5468.5 eV}. All four transitions in the XAS spectrum of the pyridine complex are slightly but consistently at higher energy than those in the XAS spectrum of the hexaaqua complex, though the difference is approximately equal to the limits of precision of the experiment. The size of the excited state 10 Dq* of these complexes was estimated to

(18) Westre, T. E.; Kennepohl, P.; DeWitt, J. G.; Hedman, B.; Hodgson, K. O.; Solomon, E. I. *J. Am. Chem. Soc.* **1997**, *119*, 6297−6314.
(19) Zhang, H. H.; Filipponi, A.; Di Cicco, A.; Lee, S. C.; Scott, M. J.; Holm, R. H.; Hedman, B.; Hodgson, K. O. *Inorg. Chem.* **1996**, *35*, 4819−4828.
(20) Fackler, J. P.; Holah, D. G. *Inorg. Chem.* **1965**, *4*, 954−958.

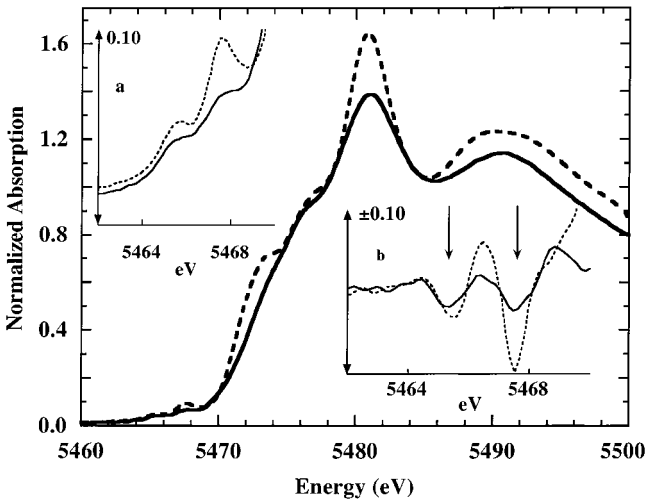

Figure 9. K-edge XAS spectra of (—) 63 mM V(II) with 2 M pyridine in 40% aqueous 1,5-pentanediol and (– – –) crystalline $[V(O_3SCF_3)_2(py)_4]$ finely dispersed in BN. Inset a: Expansion of the preedge energy region of the XAS spectra. Inset b: The second derivative of the data in inset a. Arrows mark the positions of the 1s → 3d transitions.

be about 2.3 eV from the weighted center of gravity energy differences of the two sets of two transitions.

In Figure 9 are shown the XAS spectra of crystalline $[V(O_3SCF_3)_2(py)_4]$ and of V(II) in 2 M aqueous pyridine solution. The considerations concerning the spectra of the octahedral complexes above can be applied here. The two spectra exhibit an overall congruence of observed transitions, notably in the preedge region where only two transitions of similar energy spacing appear. This is as expected in light of the EXAFS results reported above. However, the XAS spectrum of the solid complex exhibits a generally greater intensity for each transition, beginning with the preedge features near 5465 eV. Further, the intense feature at 5471 eV on the rising edge of the XAS spectrum of the crystalline tetrapyridine complex has no counterpart in the XAS spectrum of the solution complex. We have found that a similar pronounced shoulder differentiates the rising edges of the respective solid- and solution-phase XAS spectra of the hexaaqua complexes of both V(II) and V(III). Thus the XAS spectrum of crystalline $[V(H_2O)_6]SO_4$ in Figure 7 exhibits a strong shoulder at 5473 eV that is not present in the XAS spectrum of V(II) in water solution (Supporting Information Figure 3). The origin of this feature is not known but appears to have its roots in a photoelectron scattering event representative of the crystalline phase.

In the preedge region, the two transitions clearly evident (Figure 9, insets a and b) are in direct contrast with the case of the two octahedral complexes discussed above. The structure[1] of the crystalline tetragonal complex $[V(O_3SCF_3)_2(py)_4]$ indicated two close oxygens at 2.128 ± 0.001 Å, and four pyridine nitrogen ligands at 2.187 ± 0.013 Å. Two short oxygens and four longer nitrogens were also found[6] in the complex [V(saccharinate)$_2$(py)$_4$] in which each saccharinate is bound to V(II) through the imidate oxygen, with V−O = 2.071 Å and $V-N_{py} = 2.184 \pm 0.015$ Å. Interestingly, when the O/N multiplicity of ligands is reversed in the complex [V(saccharinate)$_2$(H$_2$O)$_4$], the V−O distance remains the shorter. The $V-N_{sac}$ amidate bonds are each 2.150 Å, and the four $V-O_{av}$ bonds are 2.122 ± 0.002.

In light of the discussion of the octahedral complexes above, the two preedge XAS features of the crystalline tetrapyridine complex of Figure 9 are consistent with the 1s → $^5E_{2g}$ and 1s → $^5T_{2g}$ transitions expected for an excited state of octahedral symmetry (cf. Figure 5). Because the relative degeneracies of the states are reflected in the relative intensities of the transitions, the 1s → $^5E_{2g}$ transition can be assigned to the feature at 5465.5 eV and the 1s → $^5T_{2g}$ transition to that at 5467.5 eV. It thus appears that there is no observable Jahn−Teller splitting of orbital excited states in $[V(O_3SCF_3)_2(py)_4]$ even though the ground state is already axially distorted.

Although the noise level of the XAS spectrum of V(II) in 2 M pyridine solution is higher than that of the crystalline tetrapyridine complex, the resolution is good enough to support a similar analysis. Only two preedge features are seen in the XAS spectrum (Figure 9, inset b). In analogy with the foregoing, the 1s → $^5E_{2g}$ transition can be assigned to the feature at 5465.2 eV and the 1s → $^5T_{2g}$ transition to that at 5467.4 eV. Thus, in direct contrast to the octahedral hexaaqua and hexapyridine complexes discussed above, the XAS excited states of both tetragonal complexes appear to be more symmetrical than the ground states. The virtual overlay in the energies and multiplicities of the XAS preedge features of the solution complex with those of the crystalline tetrapyridine complex is consistent with a near identity in ligand type and symmetry, and corroborates the finding obtained from the fit to the EXAFS indicating that in 2 M pyridine solution V(II) is surrounded by 4 ± 1 pyridine ligands.

Discussion

We turn now to the problem of cooperativity in pyridine binding by V(II), as described above. As noted previously, the respective K_1 values of pyridine and isonicotinamide for $[V(aq)]^{2+}$ follow the trend of pK_a and not of π-accepting ability. Figure 10 shows the $E_{1/2}$ as measured by Ghosh et al.[1] for the series of $[V(py')_4]^{2+}$ complexes (py′ = ethyl-isonicotinate, pyridine, or 4-ethylpyridine) plotted in a double-y format against both the pK_a of the ligand and the Hammett σ-meta or σ-para of the pyridine substituent. The stability of the V(II) redox co-varies directly with the electron-withdrawing strength of the substituent and in opposition to the basicity of the ligand. This correlation again reveals that metal-to-ligand dπ−pπ back-bonding plays a part in the stability of the tetrapyridine complexes. However, because this interaction is apparently absent in the initial bonding step as indicated by the K_1 values, it must arise at a later stage in the sequential ligation of $[V(aq)]^{2+}$.

This analysis can be carried further. Table 2 shows a compilation of metal−nitrogen bond lengths for the known crystal structures of the tetrapyridine complexes of V(II), and of Fe(II), which are all high-spin.[21] The Shannon−

(21) Haynes, J. S.; Rettig, S. J.; Sams, J. R.; Thompson, R. C.; Trotter, J. *Can. J. Chem.* **1986**, *64*, 429−441.

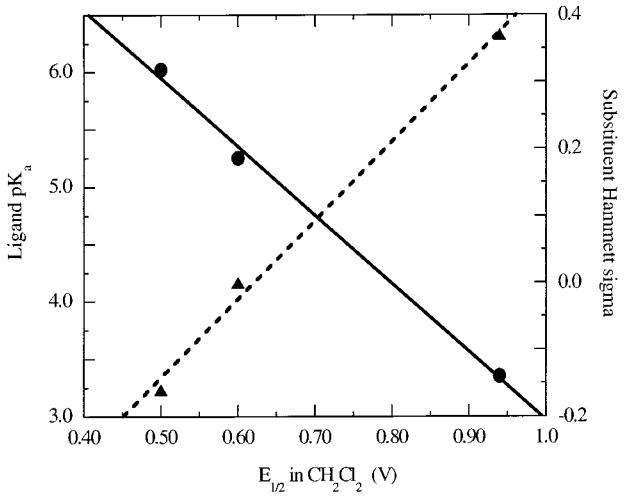

Figure 10. The redox potential of $[V(4\text{-ethylpyridine})_4]^{2+}$, $[V(\text{pyridine})_4]^{2+}$, and $[V(\text{isonicotinamide})_4]^{2+}$ in CH_2Cl_2 solution plotted as a function of (—) ligand pK_a and (− − −) the Hammett σ-para or σ-meta (as appropriate) of the pyridine substituent. The ligand pK_a values were taken from the work of Perrin,[52] and the Hammett values from that of Johnson.[53] The lines are linear least-squares fits, with $r = 0.996$ and $r = 0.995$, respectively.

Table 2. Structures of Tetrapyridine Complexes of V(II) and Fe(II)

complex	M(II)−N$_{av}$ (Å)	disposition[a]	ref
$[V(O_3Spy)_2(py)_4]$[b]	2.19 ± 0.005	propeller	49
$[V(\text{saccharinate})_2(py)_4]$	2.184 ± 0.021	propeller	6
$[V(O_3SCF_3)_2(py)_4]$	2.187 ± 0.013	propeller	1
$[VCl_2(py)_4]$	2.188[c]	propeller	50
$[FeCl_2(py)_4]$	2.246 ± 0.010	propeller	51
$[Fe(O_3SCF_3)_2(py)_4]$	2.208 ± 0.014	propeller	21
$[Fe(O_3SCH_3)_2(py)_4]$	2.228 ± 0.019	propeller	21
$[Fe(O_3Stol)_2(py)_4]$	2.228 ± 0.019	propeller	21
$[Fe(py)_6][Fe_4(CO)_{13}]$	2.257 ± 0.024	3 ⊥ planes[d]	39

[a] The rotational disposition of the four pyridine ligands with respect to the *z*-axis. [b] "O_3Spy" is pyridine-3-sulfonate; "O_3Stol" is *p*-toluenesulfonate. [c] Four identical distances are reported. [d] The six trans-coplanar pyridines are arranged along the three mutually perpendicular axes.

Prewitt ionic radii of these two metal ions[15] are nearly identical, at 0.91 and 0.93 Å, respectively. However, from the data compiled in Table 2, the average V(II)−N bond length is 2.187 ± 0.003 Å and that of Fe(II)−N is 2.228 ± 0.016 Å. The difference of 0.041 Å in favor of Fe(II) is opposed to the expectations based on the respective ionic radii, and is almost 3 times larger than the standard deviation in average Fe(II)−N bond length. This disparity is highlighted by comparing the average Fe(II)−OH_2 bond length of 2.123 ± 0.016 Å, as taken from five different $[Fe(H_2O)_6]^{2+}$ structures[22−26] with the V(II)−OH_2 bond length of 2.131 ± 0.011 Å in $[V(H_2O)_6]SO_4$.[6] Water ligands are pure σ-donors, and here the bond lengths are nearly identical and follow the Prewitt−Shannon prediction almost exactly. If the bond-length expectation from the difference in Shannon radii is included in our difference calculation, the V(II)−N bond lengths average about 0.06 Å shorter than expected, given the values of the Fe(II)−N lengths as standard. This contraction should be compared to the 0.14 ± 0.01 Å V−O bond length difference between $[V(H_2O)_6]^{2+}$ (2.131 ± 0.011 Å)[6] and $[V(H_2O)_6]^{3+}$ (1.995 ± 0.003 Å).[27,28] That is, the 0.06 Å shortening in the expected $[V(py)_4]^{2+}$ bond length is nearly half that resulting from a full unit increase in oxidation state of vanadium with σ-only donor ligands. Because all the iron(II)−tetrapyridine complexes are high-spin, it can be concluded that metal-to-ligand back-bonding does not play a large role in stabilizing these molecules. In contrast, the reduction of the V(II)−N bond distances relative to the Fe(II) standard indicates that M→L back-bonding is present in tetrapyridine V(II). Thus, three lines of evidence indicate that the back-bonding that is absent in the monopyridine V(II) complex is strongly present in the tetrapyridine V(II) complex. We suggest that the late emergence of back-bonding is the source of the cooperativity observed in the reaction of V(II) with pyridine.

The unique back-bonding in $[V(py)_4]^{2+}$ likely resides in the much greater reducing power of V(II) over that of Fe(II) ($\Delta E° = 1.03$ V), despite their similar ionic radii and charge density. This idea is consistent with the findings from infrared spectroscopic experiments on a series of transition metal $[M(L)_3]^{n+}$ complexes ($n = 3+$ to $1-$), with L = bipyridine[29,30] or *o*-phenanthroline,[29] indicating that back-bonding into the ligands increases with reduction of the metal down to the $1-$ valence state. Titanium $3+$ is a strong reducing agent but can undergo no spin change because it includes only one d electron. Nevertheless the first two stepwise additions of *o*-phenanthroline to Ti^{3+} apparently proceed cooperatively, with $K_1 = 5.39 \times 10^3$ M^{-1}, $K_2 = 3.64 \times 10^4$ M^{-1}, and $K_3 = 1.6 \times 10^4$ M^{-1}.[31] In this case, it is difficult to ascribe the onset of cooperativity to anything except increasing M→L back-bonding. The ligand 2,2′-bipyridine binds much more weakly to Ti^{3+} and shows no cooperativity,[32] likely reflecting the relative π acidity of the ligands. This is borne out by the log β_3 values governing the respective $[Fe(L)_3]^{2+}$ complexes, being 21.14 for L = *o*-phenanthroline but 17.45 for L = 2,2′-bipyridine[2] and by the values of $E°'$ for the $[Fe(L)_3]^{2+/3+}$ couples, which are 1107 and 1074 mV, respectively.[33] Further to the matter at issue, the one-electron $E_{1/2}$ for reduction of LH^+ is −970

(22) Strouse, J.; Layten, S. W.; Strouse, C. E. *J. Am. Chem. Soc.* **1977**, *99*, 562−572.
(23) Ruiz-Valero, C.; Monge, A.; Gutierrez-Puebla, E.; Gutierrez-Rios, E. *Acta Crystallogr., Sect. C: Cryst. Struct. Commun.* **1984**, *C40* (5), 811−812.
(24) Hamalainen, R.; Turpeinen, U. *Acta Chem. Scand.* **1989**, *43*, 15−18.
(25) Laine, P.; Gourdon, A.; Launay, J.-P. *Inorg. Chem.* **1995**, *34*, 5138−5149.
(26) Do, J.; Wang, X.; Jacobson, A. J. *J. Solid State Chem.* **1999**, *143*, 77−85.
(27) Cotton, F. A.; Fair, C. K.; Lewis, G. E.; Mott, G. N.; Ross, F. K.; Schultz, A. J.; Williams, J. M. *J. Am. Chem. Soc.* **1984**, *106*, 5319−5323.
(28) Beattie, J. K.; Best, S. P.; Skelton, B. W.; White, A. H. *J. Chem. Soc., Dalton Trans.* **1981**, 2105−2111.
(29) Saito, Y.; Takemoto, J.; Hutchinson, B.; Nakamoto, K. *Inorg. Chem.* **1972**, *11*, 2003−2011.
(30) Koenig, E.; Lindner, E. *Spectrochim. Acta, Part A* **1972**, *28*, 1393−1403.
(31) Tserkovnitskaya, I. A.; Novikova, E. I. *Zh. Anal. Khim.* **1969**, *24*, 1160−1164.
(32) Tserkovnitskaya, I. A.; Novikova, E. I. *Izv. Vyssh. Ucheb. Zaved., Khim. Tekhnol.* **1970**, *13*, 814−815.
(33) Szentimay, R.; Yeh, P.; Kuwana, T. Evaluation of Mediator-Titrants for the Indirect Coulometric Titration of Biocomponents. In *Electrochemical Studies of Biological Systems*; Sawyer, D. T., Ed.; American Chemical Society: Washington, DC, 1977; Vol. 38, pp 143−169.

mV for L = 2,2′-bipyridine but is −850 mV for L = *o*-phenanthroline.[34]

Finally, we return to the point raised earlier, namely, that maximal M→L back-bonding would be achieved if all four pyridine ligands were coplanar. This preferred state is not attained in crystalline $[V(CF_3SO_3)_2(py)_4]$, wherein the pyridine ligands occupy a propeller conformation. We considered the possibility that net stabilizing pyridine−pyridine interactions might attend this conformation. These could only emerge when more than one pyridine ligand is bound, and could produce a synchronous late appearance of cooperativity in pyridine binding by V(II), which latter is in fact observed. We therefore here consider the possibility that a late-emergent pyridine−pyridine interaction, rather than back-bonding, could be the source of the observed cooperativity.

In Table 2, we show that the four pyridine ligands in all structurally known V(II) and Fe(II) tetrapyridines are in a propeller configuration about the central metal. This configuration is not sterically imposed, because in a number of tetragonal transition metal complexes with even relatively large axial ligands, pyridine is known to rotate freely about the $M-N_{py}$ bond with a rotational correlation time in picoseconds.[35−37] In the propeller disposition, the pyridines are tilted about 45° with respect to the N_4 $x-y$ plane, and the molecular planes of the *trans*-pyridines are at about 90° with respect to one another. Because this arrangement is invariant and because back-bonding is apparently not important in the Fe(II) complexes, the disposition of the pyridine ligands is not preferred due to an enhanced stability induced by back-bonding. That back-bonding is apparently present in the V(II) complexes but not in the Fe(II) complexes, then, can be assigned to bonding characteristics unique to the metal and not to a special accommodation by the ligands.

In examining the question of pyridine−pyridine interactions it is necessary to distinguish attractive from repulsive contacts. To do this, we compare the ligand−ligand separations in the respective tetra- and hexapyridine complexes. For this comparison, a van der Waals radius of 1.17 Å was used for hydrogen, and of 1.08 Å for the C−H bond length.[38] The C−C van der Waals contact distance between edge-to-face perpendicular pyridine rings is then about 4.0 Å and is about 4.5 Å between $x-y$ coplanar rings. In the one known $[Fe(py)_6]^{2+}$ salt[39] (Table 2), the six pyridines are disposed in three mutually perpendicular planes and the *trans*-pyridines are coplanar. This arrangement minimizes ligand−ligand steric interactions, but obviates a strong M→L back-bonding interaction because no bonding FeN_4 molecular orbital is possible. In $[Fe(py)_6]^{2+}$ the distance between the liganding nitrogen and the α-carbon of the adjoining *cis*-pyridine ring (C'_α) averages 3.16 Å, the cis $C_\alpha-C'_\alpha$ distance between adjoining rings averages 3.64 Å, and the inter-ring torsional angle is 90°. For the Fe(II) tetrapyridines the triflate salt is representative. These distances are $N-C'_\alpha = 3.38$ Å, and $C_\alpha-C'_\alpha = 3.55$ Å, and the average inter-ring torsional angle is 79.6° ± 3.2°. The corresponding distances and angles between adjoining pyridines in $[V(O_3SCF_3)_2(py)_4]$ are $N-C'_\alpha = 3.37$ Å and $C_\alpha-C'_\alpha = 3.56$ Å, with an inter-ring torsional angle of 80.0° ± 2.5°. The tilt angles of the pyridine planes are close to 45° with respect to the N_4 plane. The dimensions within the V(II) and Fe(II) complexes are thus identical within error despite the shorter V(II)−N bond lengths. For comparison, the van der Waals distance for stacked benzene rings is 3.54 Å,[40] making all the $N-C'_\alpha$ distances sterically significant, but the $C_\alpha-C'_\alpha$ distances sterically neutral. However, if all the pyridine planes were parallel to the *z*-axis in a hypothetical pure D_{4h} $[V(py)_4]^{2+}$ molecule, the $C_\alpha-C'_\alpha$ distances would be 4.26 Å and the steric interactions between the rings would be minimized. In $[Fe(py)_4]^{2+}$, the analogous *z*-parallel pyridine−pyridine distance would be 4.39 Å. Thus, in both complexes, the pyridine−pyridine contacts are 0.7−0.8 Å closer than the available geometries require, but are similar to the ring−ring contacts in crystalline aromatic solids (see below). Because the contacts in the tetrapyridine complexes are in opposition to expectations based on minimized steric interactions, they are suggestive that the propeller arrangement of the pyridine ligands is net stabilizing.

This possibility is strengthened by consideration of the intermolecular contacts in crystalline pyridine,[41] which features herringboned stacks and nearly coplanar pyridines (173.7°). Within the stacks there is an interaction between the C−H edge of one pyridine and the central π cloud of the adjoining pyridines. The closest $N-C'_\gamma$ intermolecular contact is about 3.7 Å. In pyridine−HF the herringbone stacks include adjoining C−H edge−π cloud interactions of 3.87 Å.[42] For a variety of crystalline pyridines the intermolecular confacial van der Waals contact distance averages 3.50 Å, and can be as low as 3.17 Å in substituted molecules.[43] These distances are very similar to the $C_\alpha-C'_\alpha$ distances described above for the M(II) tetrapyridines.

The motif including interaction of the C−H edge of one aromatic molecule with the π cloud of a neighboring aromatic molecule is also found in crystalline benzene itself,[44] typifies aromatic−aromatic interactions in protein molecules,[45] and is ubiquitous in crystalline aromatic solids where it represents an energetic minimum.[38,43] These observations are understood in terms of the results of molecular orbital evaluations of various aromatic molecules including pyridine[46,47] and of Fe(II)−py[48] that show a C^--H^+ dipole

(34) Wardman, P. *J. Phys. Chem. Ref. Data* **1989**, *18*, 1637−1755.
(35) Mignot, P.; Grivet, J. P. *Chem. Phys.* **1976**, *15*, 261−267.
(36) Wada, M.; Sameshima, K. *J. Chem. Soc., Dalton Trans.* **1981**, 240−244.
(37) Huet, J.; Gaudemer, A. *Org. Magn. Reson.* **1982**, *20*, 4−10.
(38) Gavezzotti, A.; Desiraju, G. R. *Acta Crystallogr. B* **1988**, *44*, 427−434.
(39) Doedens, R. J.; Dahl, L. F. *J. Am. Chem. Soc.* **1966**, *88*, 4847−4855.
(40) Bondi, A. *J. Phys. Chem.* **1964**, *68*, 441−451.
(41) Mootz, D.; Wussow, H.-G. *J. Chem. Phys.* **1981**, *75*, 1517−1522.
(42) Boenigk, D.; Mootz, D. *J. Am. Chem. Soc.* **1988**, *110*, 2135−2139.
(43) Glówka, M. L.; Martynowski, D.; Kozlowska, K. *J. Mol. Struct.* **1999**, *474*, 81−99.
(44) Bacon, G. E.; Curry, N. A.; Wilson, S. A. *Proc. R. Soc. London, Ser. A* **1964**, *279*, 98−110.
(45) Burley, S. K.; Petsko, G. A. *Science* **1985**, *229*, 23−28.
(46) Almlöf, J.; Roos, B.; Wahlgren, U. *J. Electron Spectrosc. Relat. Phenom.* **1973**, *2*, 51−74.

and excess π-cloud electron density present in both the free and the bound pyridine molecule.

With these considerations in mind, we suggest that the propeller array so ubiquitous in the metal tetrapyridines reflects a dipolar ligand−ligand interaction analogous to those observed between aromatic molecules in crystalline solids and in proteins. Compared to the configuration in which each of the four pyridine ligands maintains a molecular plane parallel with the *z*-axis, the propeller arrangement allows the two C−H edges of every pyridine ligand to interact with the π centroid of each of the two adjoining pyridines.

Such interligand dipole interactions should lower the total energy of the $[M(py)_4]^{2+}$ molecule by an amount similar to that calculated for polyaromatic hydrocarbons,[38] which show a linear correlation between association energy and molecular size having a slope of about −1 kJ per mole per π electron. The six π electrons of pyridine should then produce an interaction stabilizing the molecule by about −6 kJ, or nearly the energy of a hydrogen bond for each of the eight pyridine−pyridine contacts in the Fe(II) and V(II) tetrapyridines, and by analogy in other $[M(py)_4]^{n+}$ complexes. If these considerations are correct, a calculational check comparing the energies of propellered vs adjoining *xz*−*yz* perpendicular pyridines should show a net favorable energetic outcome for the former. However, the emergence of pyridine−pyridine interactions on binding multiple pyridine molecules cannot be the source of the cooperativity exhibited by V(II) because the same interaction should surface during the assembly of $[Fe(py)_4]^{2+}$, which does not occur cooperatively.

To summarize and complete this picture, a late-emerging cooperativity is evident in the successive binding of pyridine by $[V(aq)]^{2+}$. The correlations of the V(II)/V(III) $E_{1/2}$ in $[V(py')_4]^{2+}$ complexes with Hammett σ parameters and ligand pK_a values and the 0.06 Å contraction of the M(II)−N bond lengths in $[V(py)_4]^{2+}$ relative to $[Fe(py)_4]^{2+}$ indicate that metal−ligand dπ−pπ back-bonding is uniquely important in the V(II) complexes. The propeller arrangement of pyridine ligands in the V(II) and Fe(II) tetrapyridine complexes is proposed to be due to an edge-to-centroid dipolar interaction between adjoining pyridine ligands, which is here suggested to be present in all other propeller-disposed $[M(py)_4]^{n+}$ complexes. The ligand−ligand stabilization energies proposed to arise in the tetrapyridine complexes cannot be the source of the cooperativity in the reaction of V(II) with pyridine, however, because of the absence of any analogous cooperativity in the reaction of Fe(II) with pyridine. This disparity again implicates the late emergence of V(II)→pyridine back-bonding—not appearing until after the first ligand is bound—as the only remaining causal candidate for the cooperative binding of pyridine by V(II). This conclusion is reinforced by the cooperativity exhibited in the reaction of Ti^{3+} with *o*-phenanthroline, noted above. That cooperativity in the V(II)−pyridine system is not accompanied by a spin change excludes ligand-induced spin pairing from the status of sine qua non with respect to cooperative ligand binding in first-row divalent transition metals.

Acknowledgment. This work was supported by Grants NSF CHE 94-23181 and NIH RR-01209 (to K.O.H.) and by NSF CHE-97-27416 (to H.T.). XAS data were collected at SSRL, which is supported by the Department of Energy, Office of Basic Energy Sciences, Divisions of Chemical and Materials Sciences. The SSRL Biotechnology Program is supported by the National Institutes of Health, National Center for Research Resources, Biomedical Technology Program, and by the Department of Energy, Office of Biological and Environmental Research.

Supporting Information Available: Figures depicting titrations of pyridine and isonicotinamide in water with increasing V(II) and vanadium K-edge XAS spectra of $[V(H_2O)_6]SO_4$. This material is available free of charge via the Internet at http://pubs.acs.org.

IC011221O

(47) Palmer, M. H.; Findlay, R. H.; Gaskall, A. J. *J. Chem. Soc., Perkin Trans. 2* **1974**, 420−428.
(48) Clack, D. W.; Kane-Maguire, L. A. P.; Knight, D. W.; Williams, P. A. *Transition Met. Chem.* **1980**, *5*, 376−378.
(49) Cotton, F. A.; Daniels, L. M.; Montero, M. L.; Murillo, C. A. *Polyhedron* **1992**, *11*, 2767−2774.
(50) Brauer, D. J.; Krueger, C. *Cryst. Struct. Commun.* **1973**, *2*, 421−426.
(51) Long, G. J.; Clark, P. J. *Inorg. Chem.* **1978**, *17*, 1394−1401.
(52) Perrin, D. D. *Dissociation Constants of Organic Bases in Aqueous Solution*; Butterworth & Co. LTD: London, 1965.
(53) Johnson, C. D. *The Hammett Equation*; Cambridge University Press: Cambridge, 1973.